universe

MDPI

Review

Fluctuations and Correlations of Conserved Charges Serving as Signals for QGP Production: An Overview from Polyakov Loop Enhanced Nambu–Jona-Lasinio Model

Sudipa Upadhaya

Ramsaday College, Amta, Howrah 711401, West Bengal, India; sudipa.09@gmail.com

Abstract: Quark–Gluon plasma driven by the strong force is subject to the conservativeness of the baryon number, net electric charge, strangeness, etc. However, the fluctuations around their mean values at specific temperatures and chemical potentials can provide viable signals for the production of Quark–Gluon plasma. These fluctuations can be captured theoretically as moments of different orders in the expansion of pressure or the thermodynamic potential of the system under concern. Here, we look for possible explanations in the methodologies used for capturing them by using the framework of the Polyakov–Nambu–Jona-Lasinio (PNJL) model under the 2 + 1 flavor consideration with mean-field approximation. The various quantities thus explored can act to signify meaningfully near the phase transitions. Justifications are also made for some of the quantities capable of serving necessarily under experimental scenarios. Additionally, variations in certain quantities are also made for the different collision energies explored in the high-energy experiments. Rectification of the quantitative accuracy, especially in the low-temperature hadronic sector, is of prime concern, and it is also addressed. It was found that most of the observables stay in close proximity with the existing lattice QCD results at the continuum limit, with some artifacts still remaining, especially in the strange sector, which needs further attention.

Keywords: quark–gluon plasma; PNJL model; fluctuations; correlations

check for updates

Citation: Upadhaya, S. Fluctuations and Correlations of Conserved Charges Serving as Signals for QGP Production: An Overview from Polyakov Loop Enhanced Nambu–Jona-Lasinio Model. *Universe* **2024**, *10*, 332. https://doi.org/10.3390/universe10080332

Academic Editors: Souvik Priyam Adhya, Sandeep Chatterjee, Sreemoyee Sarkar and Claudia Ratti

Received: 30 April 2024
Revised: 11 August 2024
Accepted: 13 August 2024
Published: 19 August 2024

Copyright: © 2024 by the author. Licensee MDPI, Basel, Switzerland. This article is an open access article distributed under the terms and conditions of the Creative Commons Attribution (CC BY) license (https://creativecommons.org/licenses/by/4.0/).

1. Introduction

At high temperatures and densities, strongly interacting matter is expected to witness a transition from the confined state, the hadronic phase, to a deconfined partonic state, where the restoration of chiral symmetry occurs in conjunction with the deconfinement of quarks [1–5]. In order to understand the fundamental interactions in physics, as well as to have a thorough insight into the early universe and neutron stars, it is very important to understand the phenomena involved. To this end, research on the existence of a possible second-order phase transition is currently ongoing, with studies working toward the conjecture of the possible location of the critical end point (CEP). It is thus important to study and investigate observables, which give a signal of the transition from one phase to the other. Fluctuations in the baryon number, electric charge, and strangeness act as such viable signals. The D-measure, for example, expressed in terms of the fluctuations of the net electric charge, gives one such possible signal [6–8]. This quantity takes up distinctly unique values for the hadronic and partonic phases, thus resulting in the excellent signaling of the transition from one phase to the other. In the experimental scenario, the heavy-ion collisions are measurable with an event-by-event (EbE) analysis [9,10], with each event corresponding to a collision.

In this context, various studies are being performed on the theoretical and experimental fronts in search of the critical end point. The framework of the lattice QCD gives a benchmark estimate for the computational baseline [11–29]; however, QCD-inspired models are proving to be eligible candidates, barring the complexities of the lattice at non-zero chemical potentials. They are found to be highly useful in describing the different

attributes of strongly interacting matter at different temperatures and chemical potentials. One such model is the Polyakov–Nambu–Jona-Lasinio or the PNJL model. This model was formed by appending the Polyakov or P-loop to the NJL model [30–32]. The NJL, or the Nambu–Jona-Lasinio model, was formed with the global symmetries of the QCD-like chiral symmetry. The multiquark interaction terms give rise to dynamic fermion mass generation, which leads to spontaneous chiral symmetry breaking. However, since the gluon degrees of freedom are integrated at this point, the model fails to incorporate the crucial feature of confinement. This is where the PNJL model, by adding the background gluon field, gives a sense of confinement, thus incorporating the two important transitions of chiral symmetry breaking and its restoration and the confinement–deconfinement transition into a single framework [33–39]. The various parameters in this model are fixed by adhering to the lattice scenario. The PNJL results showed a satisfactory qualitative agreement with the lattice results. The latter lattice findings were for finite lattice spacings. The lattice QCD data, in the recent past, have been extrapolated to the continuum limit [40], and they have obtained continuum extrapolations for a number of observables. However, the previously obtained PNJL results were rendered incapable of showing the close proximity to the recently obtained lattice continuum data. Henceforth, it became a mandate that the PNJL model parameters were set to show good quantitative agreement with the lattice. Following this, the parameters in the PNJL model were re-set, such that the transition temperature T_c matched with the lattice and also such that the temperature dependence of the pressure was in close conjunction with the lattice. It is also important to check the other derivatives of the pressure and contrast them with the lattice results. For the physical case of two light strange quarks and one heavier strange quark, the crossover temperature was reported by the Hot-QCD and Wupertal–Budapest collaborations [40–45] to be in the range of 150–160 MeV. The corresponding readjustment of the Polyakov loop potential brought about a satisfactory overall agreement between the PNJL and lattice results; however, the match was far from perfect. A main region of disagreement was in the low-temperature regime, where the hadronic degrees of freedom played a major role. This was expected, though, since this regime was not yet adequately addressed in the PNJL model. In this context, it needs to be mentioned that the Hadron Resonance Gas (HRG) model [46–52] has given excellent results in the hadronic sector in central heavy-ion collisions, ranging from the Alternating Gradient Synchrotron (AGS) up to the Relativistic Heavy-Ion Collider (RHIC) energies [53,54]. It is also noteworthy that the susceptibilities of the conserved charges calculated using the background of the lattice QCD have been excellently reproduced by the HRG model for temperatures up to 150 MeV [55]. The regime of high chemical potentials below the critical region can be studied using this model. Henceforth, it is established that the HRG model is quite suitable for describing the hadronic phase of the strong interactions. The HRG model, which is based on the theorem of Dashen, Ma, and Bernstein, illustrates that the dilute system of strongly interacting matter can be described by the gas of free resonances. Though these resonances take care of the long-range attractive part of the hadron interactions, they are incapable of addressing the short-range repulsion, which is also very important for describing the strongly interacting matter. Upon close approach to the critical or crossover regime, the HRG calculations tend toward Hagedorn divergence, which is possibly due to the absence of repulsive interactions.

It is thus of urgent importance to obtain a single model that addresses both the low- and high-temperature domains effectively. This can be achieved by creating an interface between one model, which is appropriate for the partonic phase, and another one for the hadronic phase. This approach is well taken care of by using a switching function to club the HRG and PNJL models. The switching function is crucial for two reasons. Firstly, it is necessary to consider the hadronic contribution at low temperatures, which is missing in the PNJL model. Secondly, at high temperatures, the partonic contribution dominates, and thus hadronic ones need to be suppressed in that regime. On the contrary, at low temperatures, the partonic contribution is already suppressed, thus making the switching function superfluous in this regime. The switching function should be designed to give

the correct proportion of the hadronic and partonic contributions. This gives an indeed effective way where by clubbing the two models, good realization of the entire picture is achieved.

An alternative and a more internal way to address the same issue is where the hadronic contributions are added in a simple manner while considering their medium-dependent masses. Using the Polyakov loop, the confinement feature always suppresses the contributions of the constituent quarks at low temperatures and densities. In the former case, the switching function was crucial to cut-off the hadronic contributions at high temperatures and densities. Here, in this case, instead of using an external switching function, the increasing effective masses of hadrons will act as natural in-built switching functions. Thus, the quantitative accuracy is also achieved. This should further aid in obtaining the fluctuations and correlations of the conserved charges in the system with higher accuracy, thus acting as viable signals for QGP production under exotic conditions.

Similar studies have also been performed under the frameworks of various QCD-inspired models like the Linear Sigma Model (LSM) [56–58] and the Polyakov Loop Linear Sigma Model (PLSM) [59–66]. These models are equivalent to the NJL or PNJL ones and bear special attention in order to analyze the different features of the matter under concern, including its transition properties, thermodynamics, and observables, to indicate phase structures. Meson masses in the scalar, pseudoscalar, vector, and axial vector channels were also explored with precision. Over the years, following works in similar directions using effective interaction models of quarks embedded in frameworks of the Schwinger–Dyson equation have contributed significantly to the community as well [67–73] in terms of predicting phase transitions and associated observations. To this end, the PNJL model has also advanced in recent years to encompass the various observations related to the phase transitions and associated symmetry patterns and to study the transport coefficients applicable in the hydrodynamic scenario, thus posing unique ways to portray the phase diagram [74–83].

2. The Model Frameworks

The Nambu-Jona—Lasinio (NJL) model takes care of the chiral properties but fails to address the confinement–deconfinement transition. To this end, the Polyakov loop-enhanced NJL or the PNJL model explains the deconfinement physics successfully. Studies have been performed using both 2 and 2 + 1 flavors considering up to six- and eight-quark interactions [84–87]. The thermodynamic potential looks like

$$\begin{aligned}\Omega = \; & \mathcal{U}'\left(\Phi[A],\overline{\Phi}[A],T\right) + 2g_S \sum_{f=u,d,s}\sigma_f^2 - \frac{g_D}{2}\,\sigma_u\sigma_d\sigma_s + 3\frac{g_1}{2}\left(\sum_f \sigma_f^2\right)^2 + 3g_2\sum_f \sigma_f^4 \\ & -6\sum_f \int_0^\Delta \frac{d^3p}{(2\pi)^3}\, E_{p_f}\Theta\left(\Lambda - \left|\vec{p}\right|\right) \\ & -2\sum_f T\int_0^\infty \frac{d^3p}{(2\pi)^3}\, ln\left[1 + 3\left(\Phi + \overline{\Phi}\, e^{-\frac{(E_{p_f}-\mu_f)}{T}}\right) e^{\frac{-(E_{p_f}-\mu_f)}{T}} + e^{\frac{-3(E_{p_f}-\mu_f)}{T}}\right] \\ & -2\sum_f T\int_0^\infty \frac{d^3p}{(2\pi)^3}\, ln\left[1 + 3\left(\Phi + \overline{\Phi}\, e^{-\frac{(E_{p_f}+\mu_f)}{T}}\right) e^{\frac{-(E_{p_f}+\mu_f)}{T}} + e^{\frac{-3(E_{p_f}+\mu_f)}{T}}\right]\end{aligned} \tag{1}$$

σ_f are the condensates corresponding to the up, down, and strange quarks. g_S and g_D are the four and six quark coupling terms, where the latter ensures axial U(1) symmetry breaking. g_1 and g_2 are the eight-quark coupling terms, which become zero in the absence of the eight quark interactions. The coupling constants are dimensionful, thereby making the theory non-renormalizable. A three-momentum ($\left|\vec{p}\right|$) cutoff scheme has therefore been

introduced and manifested by $\Theta\left(\Lambda - \left|\vec{p}\right|\right)$. $E_{p_f} = \sqrt{p^2 + M_f^2}$ is the quasiparticle energy. The constituent quark masses are given by

$$M_f = m_f - g_S\sigma_f + \frac{g_D}{2}\sigma_{f+1}\sigma_{f+2} - 2g_1\sigma_f\left(\sigma_u^2 + \sigma_d^2 + \sigma_s^2\right) - 4g_2\sigma_f^3 \tag{2}$$

where σ_f takes up corresponding values for u, d, and s quarks in a clockwise manner. The integral with finite range gives a zero-point energy, whereas the last two terms indicate the contributions of the constituent quarks in the finite temperature and chemical potential domain. They are nothing but the modified fermion determinants in the presence of the Polyakov loop field $\Phi = \frac{Tr_c L}{N_c}$ and its conjugate $\overline{\Phi} = \frac{Tr_c L^\dagger}{N_c}$, with L being the Polyakov loop given by

$$L\left(\vec{x}\right) = \mathcal{P}\text{exp}\left[i\int_0^{1/T} d\tau\ A_4(\vec{x},\tau)\right] \tag{3}$$

A_4 is the time component of the background gluonic field. The self-interaction of Φ and $\overline{\Phi}$ is described by the effective potential $\mathcal{U}'$:

$$\frac{\mathcal{U}'[\varphi,\overline{\varphi},\ T]}{T^4} = \frac{\mathcal{U}[\varphi,\overline{\varphi},\ T]}{T^4} - \kappa\ln(J[\varphi,\overline{\varphi}]) \tag{4}$$

Here, $\mathcal{U}$ is one Landau–Ginzburg type potential following the global Z(3) symmetry of the Polyakov loop given by

$$\frac{\mathcal{U}[\varphi,\overline{\varphi},\ T]}{T^4} = -\frac{b_2(T)}{2}\,\overline{\varphi}\,\varphi - \frac{b_3}{6}\left(\varphi^3 + \overline{\varphi}^3\right) + \frac{b_4}{4}\,(\varphi\overline{\varphi})^2 \tag{5}$$

The temperature dependence has been completely absorbed in the coefficient b_2 as

$$b_2(T) = a_0 + a_1\left(\frac{T_0}{T}\right) + a_2\left(\frac{T_0}{T}\right)^3 \tag{6}$$

This truncated series has later been modified to stay in close proximity with the lattice result, the modified form being [88] as follows:

$$b_2(T) = a_0 + a_1 exp\left(-a_2\frac{T}{T_0}\right)\frac{T_0}{T} \tag{7}$$

Fixing of the parameters has been detailed in [89], and the crossover temperatures were found to be 166.5 and 162.5 MeV, respectively, for six- and eight-quark frameworks, falling in line satisfactorily with the lattice findings.

The pressure is found from the thermodynamic potential, which is minimized with respect to the corresponding degrees of freedom present in the system, thereby finding the values of the associated fields. The fluctuations of conserved charges and correlations among them are found using the series expansion of the scaled pressure w.r.t the scaled chemical potential as follows:

$$c_n^X(T) = \frac{1}{n!}\,\frac{\partial^n\left(P/T^4\right)}{\partial\left(\frac{\mu_X}{T}\right)^n} = T^{n-4}\chi_n^X(T) \tag{8}$$

$$c_{m,n}^{X,Y} = \frac{1}{m!n!}\,\frac{\partial^{m+n}\left(P/T^4\right)}{\left(\partial\left(\frac{\mu_X}{T}\right)^m\right)\left(\partial\left(\frac{\mu_Y}{T}\right)^n\right)} = T^{m+n-4}\chi_{m,n}^{X,Y}(T) \tag{9}$$

The net charge fluctuation, once obtained from Equation (8), can also be used to define a quantity named D-measure, as elaborated in the following section. This, being a ratio of net charge fluctuations with total charge density, can serve as a viable quantity in the experimental scenario as well, since both of them are experimentally measurable.

On the other side, the HRG model has been quite successful in analyzing the production of hadrons in high-energy, heavy-ion experiments [90–102]. The observables under concern here are parallelly well-described [103–106] up to a temperature range of 150 MeV, i.e., the crossover region. However, the absence of repulsive interaction causes Hagedorn divergence there, which is taken care of in the Excluded Volume HRG (EVHRG) model framework [105,107–116] under acceptance ranges of transverse momentum and pseudo rapidity. It is thus also applied in the systematic hydrodynamic analysis of the system [117–119]. In this preliminary study, the goal is, however, to witness the success of incorporating hadronic degrees of freedom to elevate the results of the PNJL model in the low-temperature sector for better agreement with the existing lattice QCD results. The ideal gas of hadrons, following the Particle Data Group [120], has been used, where the grand partition function is

$$\ln\ Z^{id} = \sum_i \ln\ Z_i^{id} \tag{10}$$

Z_i^{id}, the partition function for the ith resonance particle then takes the form

$$\ln\ Z_i^{id} = \pm\frac{V g_i}{2\pi^2}\int_0^\infty p^2 dp \ln\{1 \pm exp[-(E_i - \mu_i)/T]\} \tag{11}$$

V is the volume of the system, with g_i being the degeneracy factor. $E_i = \sqrt{p^2 + m_i^2}$ is the single-particle energy, with m_i being its mass. T is the temperature, and $\mu_i = B_i\mu_B + Q_i\mu_Q + S_i\mu_S$ is the chemical potential of the ith species, formed using the corresponding chemical potentials of the conserved charges considered for this analysis. '+' and '−' signs refer to the fermions and bosons, respectively. The pressure, and hence other thermodynamic quantities, can be obtained from this partition function using the standard thermodynamic relations.

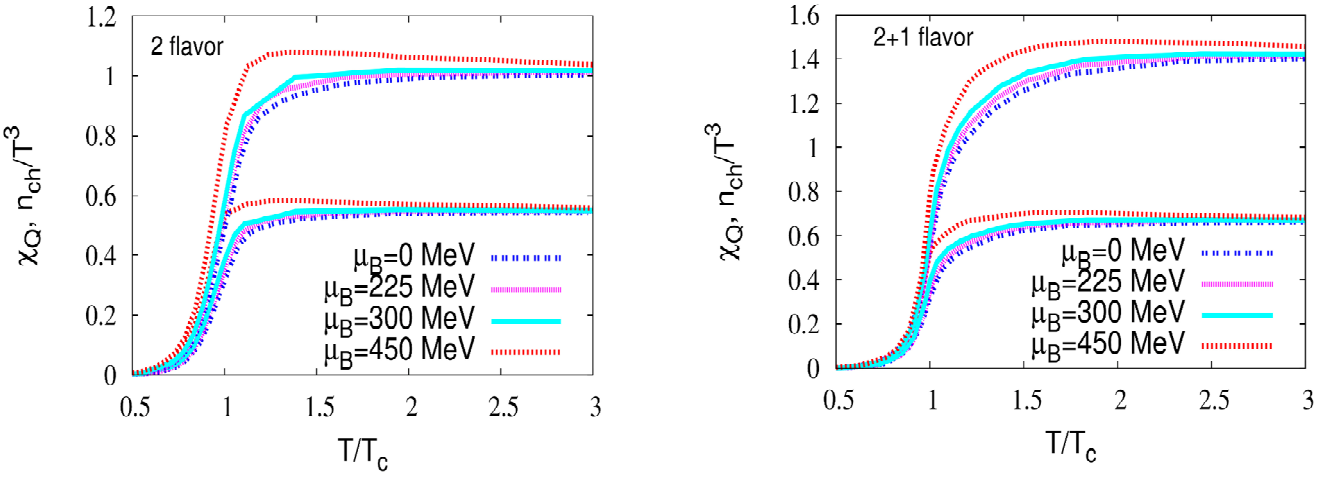
3. Results

The quantity D-measure was defined as the net charge fluctuation in a form of ratio of two experimentally measurable quantities in order to reduce systematic uncertainties. This is defined as [6] follows:

$$D = 4\ \frac{\chi_Q}{n_{ch}/T^3} \tag{12}$$

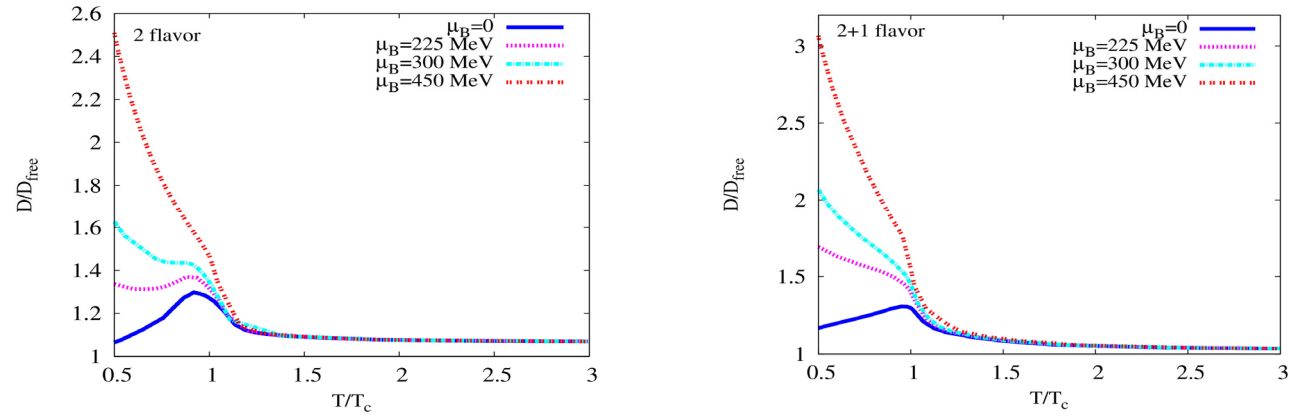
Here, χ_Q is the net electric charge fluctuation, and n_{ch} is the total charge density. χ_Q (or χ_2^Q) is calculated in a similar way as in Equation (8), i.e., in a dimensionless manner, whereas n_{ch} is obtained using the quark and antiquark distribution functions as they appear in PNJL model. As per the conserved charges considered for this study, viz., the baryon number, net electric charge, and strangeness, the corresponding chemical potentials are used to construct the chemical potentials of quarks of different flavors, $\mu_f = B_f\mu_B + Q_f\mu_Q + S_f\mu_S$. While calculating the charge fluctuations, chemical potentials for the other charges are kept constant at zero. Considering a system consisting of pion gas for the hadronic region and calculations from lattice gauge theory for the partonic phase reveals a value of D to be close to 4 and 1, respectively. D has also been measured experimentally by ALICE collaborations in a rapidity window $0.2 < \Delta\eta < 1.6$ using collision energy, $\sqrt{s} = 2.76$ TeV in a Pb-Pb run considering different centralities [89,121]. The result shows D to fall consistently with an increase in $\Delta\eta$, obeying results from UrQMD simulation. The results from the STAR collaboration are also available.

Figure 1 shows the variations of χ_Q and n_{ch}/T^3 for 2 and 2 + 1 flavor systems with temperature from the PNJL model. These are then employed to obtain D/D_{free}, where D_{free} represents the limiting value of D for a free, massless gas of quarks. This quantity is portrayed in Figure 2.



(**a**) (**b**)

Figure 1. Charge susceptibility and total electric charge density with temperature for various baryon chemical potentials. (**a**) for 2-flavor system and (**b**) for 2 + 1 flavor system. Figures are taken from [6].



(**a**) (**b**)

Figure 2. Scaled 'D' with scaled 'T' for various values of μ_B around μ_Q = 0. Figures are taken from [6]. Panels (**a**,**b**) indicate results for 2 and 2 + 1 flavor frameworks, respectively.

The results are qualitative, but clearly indicate a transition close to T~T_c. The non-monotonic behavior in the low-temperature regime accounts for the absence of explicit hadronic degrees of freedom in the model framework, which was later addressed using two methods; the first one incorporated an appropriate switching function [55] to serve as an adhesive agent between the HRG and PNJL models. The second one [122] was to use the temperature-dependent hadronic masses, thus contributing to the thermodynamic potential accordingly. The quantity D was also computed as a function of collision energy, $\sqrt{s}$, as depicted in the experimental situation, using the freeze-out parametrization [123]. This was found to fall from a higher value before getting saturated, falling in line with the experimental findings, as shown in Figure 3. As in [121], the numerical range of D and its qualitative nature agree with the findings of PNJL outcomes. However, it is to be remembered that the freezeout curve directs to states under complete thermal equilibrium and hence falls solely in the hadronic region. So, a complete match of any observable with experimental findings cannot be expected. Moreover, since considering rapidity range is beyond the scope of the framework of the PNJL model, the dynamics of such a system have not been considered in this case.

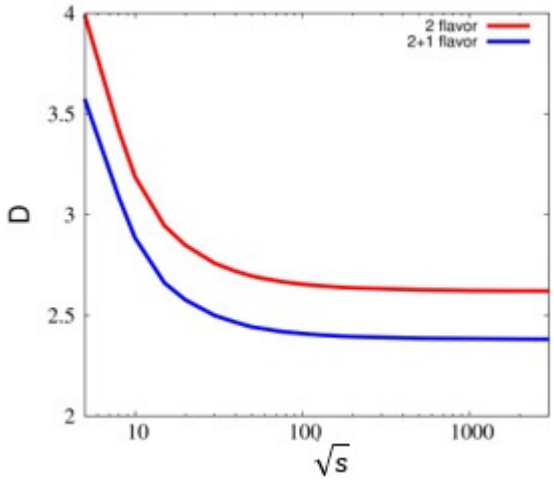


Figure 3. D with $\sqrt{s}$ along the freeze-out curve [6], where $\sqrt{s}$ is in MeV.

The baryon number and strangeness are also conserved charges, and measuring their fluctuations can be of immense importance in this regard. Figure 4 shows the variation of second- and fourth-order susceptibilities of the baryon number, named c_2^B and c_4^B, respectively [88]. The quantitative agreement with the lattice QCD data is quite encouraging; however, the mismatch becomes prominent as the order is increased.

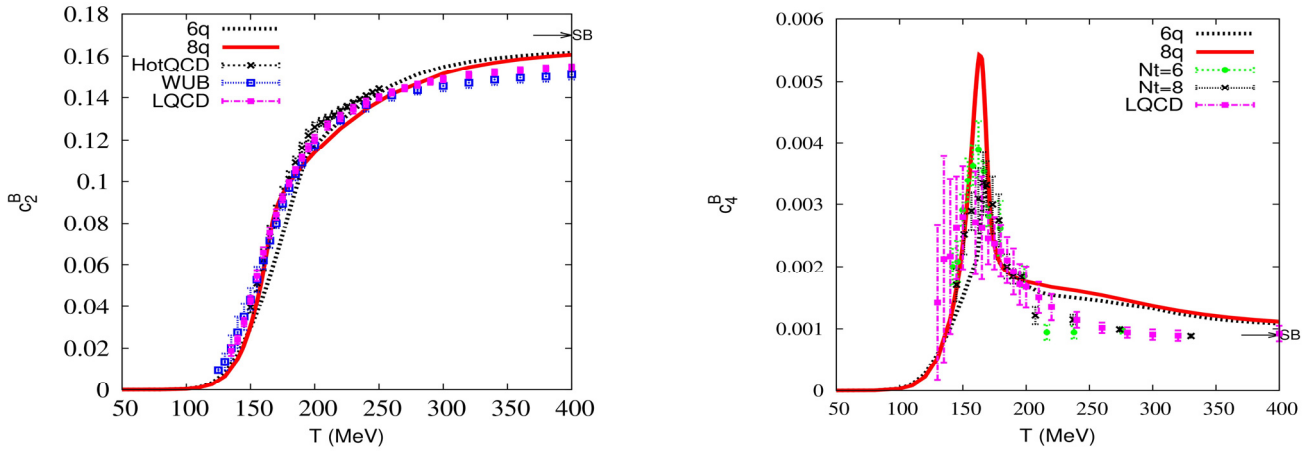


Figure 4. Baryon number susceptibilities of second and fourth order are shown in comparison to various existing lattice results. Figures are taken from [88].

Similar quantities for strangeness are shown in Figure 5. The deviation from the existing lattice results is quite noteworthy here and calls for proper modifications with the insertion of hadronic degrees of freedom in the low-temperature regime. The maxima in c_4^S is widely shifted as the melting of strange quark condensate occurs at higher temperatures as compared to the lattice case. This is an artifact in the NJL model parameters, which were fixed entirely at zero temperature and chemical potentials.

The discrepancies were somewhat addressed using a hybrid model by tagging the suitable HRG and PNJL model results using a smooth switching function of the following form [55]:

$$S(T) = \frac{1}{1 + \exp\left[-\frac{T - T_S}{\Delta T_S(T)}\right]} \tag{13}$$

which varies continuously from one phase to the other around the crossover region. Hence, this function essentially provides the necessary weightage to the HRG or PNJL model outcome

in the corresponding region of temperature. As stated previously, the absence of any single model framework to suitably describe the physics in both the partonic and hadronic sectors necessitates the use of clubbing the two relevant models in an effective manner. Such an idea was successfully implemented by using the HRG and PQCD (perturbative-QCD) results, as in [124], and also merging the HRG and IQ (Interacting Quark) models [125,126]. Considering the hadrons and partons to be states of the same underlying theory of QCD, they can appear simultaneously under some evolved thermodynamic condition of the system. The theory is thus based on a mixture of states in the crossover region, supported by the lattice-QCD results toward the crossover of hadronic dominance to partonic dominance. The coexistence of the hadronic and partonic degrees of freedom near crossover thus makes it possible to explore such frameworks [127–131]. A suitable choice of switching function would then play the role of clustering probability to create a coexisting condition for a simple mixture of the two different sets of degrees of freedom under a specific condition without any overcounting in them. The one used here in Equation (13) is thus used to choose the necessary degrees of freedom suitably in the corresponding window of temperature under concern, with no effect on underlying structures of the PNJL or HRG models and thus keeping all symmetries and their breakings intact. The phase boundary also remains solely dependent on the PNJL model. This helps in fixing the change-over temperature, T_s, close to the crossover temperature. The effects of the derivatives of the switching function while obtaining various thermodynamic quantities may have additional consequences, which, however, have not been considered after detailed investigations [55] by approximating that each observable has an individual dependence on the switching function. The other parameter $\Delta T_S(T)$ is fixed at par with the width of the crossover region, thus corresponding to a spread in the crossover temperature. The results of pressure from lattice-QCD were used for this purpose. The corresponding parameter set can be found in Table 4 of [55].

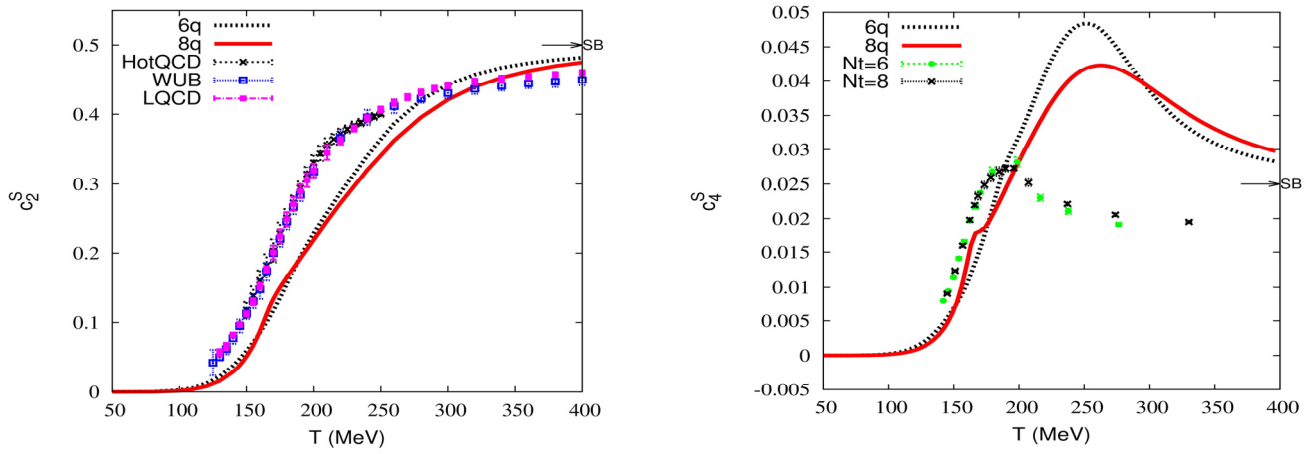


Figure 5. Second- and fourth-order strangeness susceptibilities with temperature are shown in comparison to existing lattice data [40–45]. Figures are taken from [88].

On the other hand, as specified, the medium-dependent hadronic masses can also act as built-in switching functions. The low-lying hadrons will be the dominant contributors to the pressure of the system, and hence hadrons of masses up to 1 GeV have been considered. The baryonic masses have been considered to remain fixed as they possess comparatively higher masses than the lowest-lying mesons, which are the predominant partners in this regard. The temperature-dependent mesonic masses can be found by solving the pole condition, as in [122]:

$$1 - 2G_M \Pi_M \left(\omega = m_M, \vec{k} = 0 \right) = 0$$

Here, G_M is the vertex factor for the corresponding flavor combination, and $\Pi_M(\vec{k}^2)$ is the one-loop polarization function for that mesonic channel, which can be solved using the appropriate quark propagator, as can be found in [122] and references therein. The temperature-dependent masses of mesons which have been considered are shown in Figure 6. These masses have also been studied in the frameworks of the PLSM model by different groups [59,65], and the results show satisfactory equivalence. Variations under the finite temperature and chemical potentials domain have been made in [65]. In the PNJL model, the meson masses are evaluated in the presence of the Polyakov loop fields and quark condensates, which are evaluated at present under mean field approximation, thus helping to solve the pole conditions. The PLSM model, on the other hand, concentrates on the direct attachment of associated terms in the Lagrangian system itself in the scalar, pseudoscalar, vector, and axial vector channels, thereby considering the symmetry effects [60–65]. Isospin chemical potentials have been introduced to study the phase diagram in view of the persisting scenario, and thermodynamic quantities were shown to match well with lattice QCD findings, along with the crossover temperature being in close vicinity.

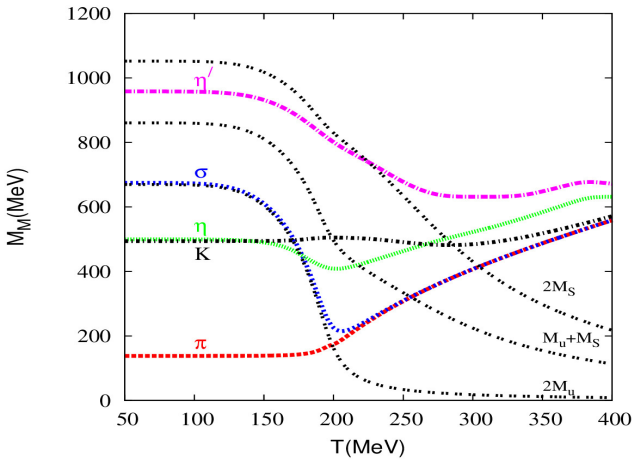


Figure 6. Temperature-dependent meson masses, as calculated using PNJL distribution function. Figure is taken from [122].

The final contribution of the mesons in the thermodynamic potential thus takes the following form:

$$\delta'\Omega_M = -\nu_M T \int \frac{d^3p}{(2\pi)^3} \ln\left(1 - e^{\frac{-E_p}{T}}\right),$$

ν_M is the corresponding weight factor for the particular meson, and $E_p = \sqrt{\vec{p}^2 + m_{pole}^2(T)}$, with m_{pole} being the corresponding mesonic mass. Similarly, the baryonic contribution to the thermodynamic potential is considered as

$$\delta'\Omega_B = \nu_B T \int \frac{d^3p}{(2\pi)^3} \ln\left(1 + e^{\frac{-E_p}{T}}\right)$$

where baryonic masses lying within 1 GeV are taken as constants. Thus, finding the full thermodynamic potential and hence the pressure, the susceptibilities can be obtained by suitably Taylor expanding and fitting for the corresponding coefficients as before. The renormalized version of the PNJL model, with medium mass modifications of the hadrons, indeed serves as one potential framework to describe the underlying physics self-consistently. This can be verified from the observed thermodynamic quantities, as portrayed in Figure 7. The previously observed discrepancies in the low-temperature segment are well

taken care of now. Figure 7 describes four observables, viz., the pressure (a), energy density (b), speed of sound (c), and specific heat (d) in the four panels, respectively. One additional discrepancy in the hybrid picture of entangling the HRG results with PNJL ones was to incorporate derivatives of the external switching function. Not only would this increase the number of parameters, but it would also have additional effects to deviate the desired scenario from the physical situation. This is also avoided in the new formalism, as can be verified from Figure 7, panels (b), (c), and (d), where derivatives of pressure are involved, yet showing satisfactory agreements with the existing results from lattice calculations.

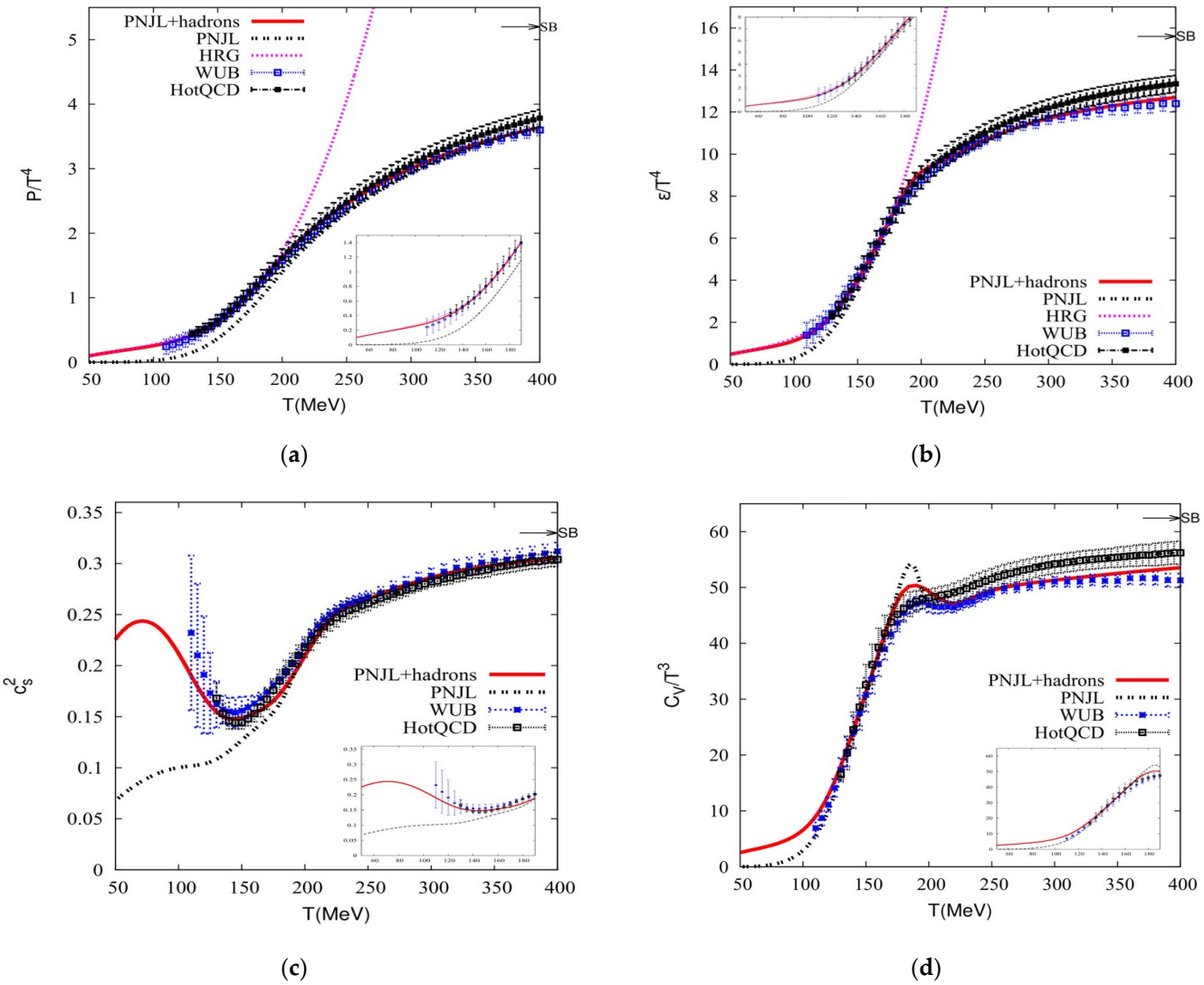
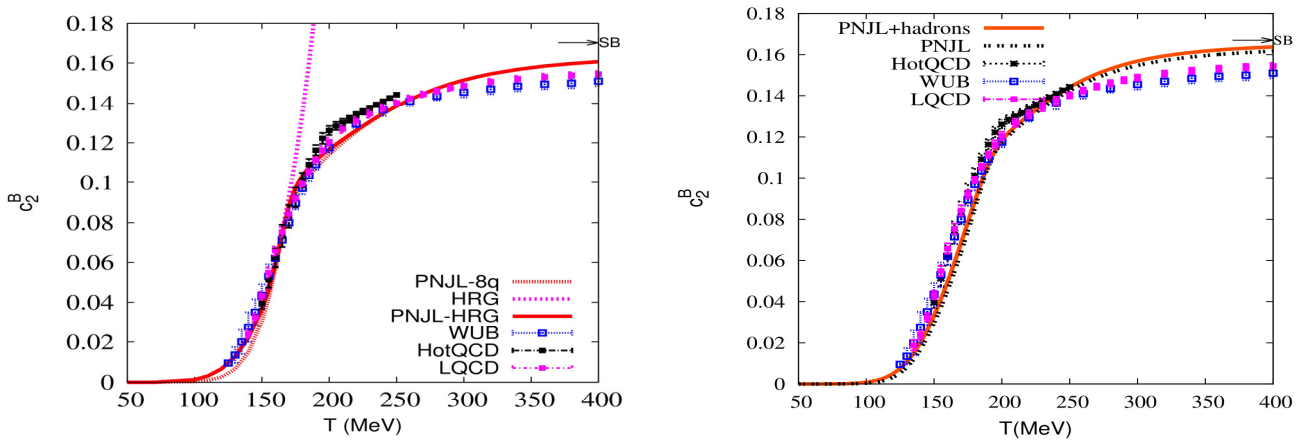


Figure 7. Thermodynamic quantities obtained from the mass-modified PNJL model. Panels show (**a**) pressure, (**b**) energy density, (**c**) speed of sound, and (**d**) specific heat with temperatures, whereas the insets indicate the zoomed-in region in the low-temperature sector.

The inset diagrams picture the zoomed-in region in the low-temperature sector, where quantitative mismatches were profound previously. This essentially boosts beyond and obtains the fluctuations and correlations among the conserved charges present in the system. Figure 8 shows the leading-order baryon number susceptibilities, as found from the hybrid and the mass-modified PNJL model. In both cases, the model shows a satisfactory match for the entire window of temperature with the lattice outcome. The HRG result matches up to the crossover region. For the hybrid model, results from 8-q-type interaction are only shown here. The PNJL outcome itself falls closely to the lattice result, as the

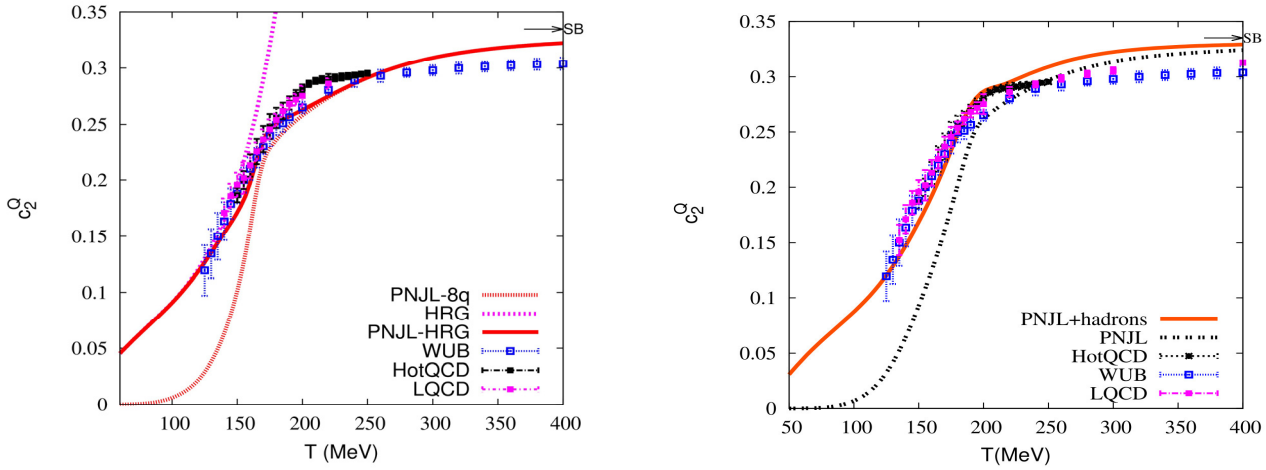
baryons are well accounted for by the constituent quarks in this model, as depicted in the distribution functions.



(**a**) (**b**)

Figure 8. Second-order baryon number susceptibilities, as obtained from (**a**) 8–quark PNJL + HRG hybrid model and (**b**) mass-modified PNJL model. Figures are taken from [55,122].

However, significant departure is observed for the electric charge fluctuations. Figure 9 portrays the results from the two different methods along with the PNJL results vis-à-vis lattice data. The mismatch was primarily in the low-temperature domain, where the absence of explicit hadrons creates deviation. The use of the HRG results and, more physically, the use of the temperature-dependent hadron masses, removes the discrepancy to a great extent and provides satisfactory matches. This is quite expected, as the charge sector is dominantly contributed by the light hadrons.

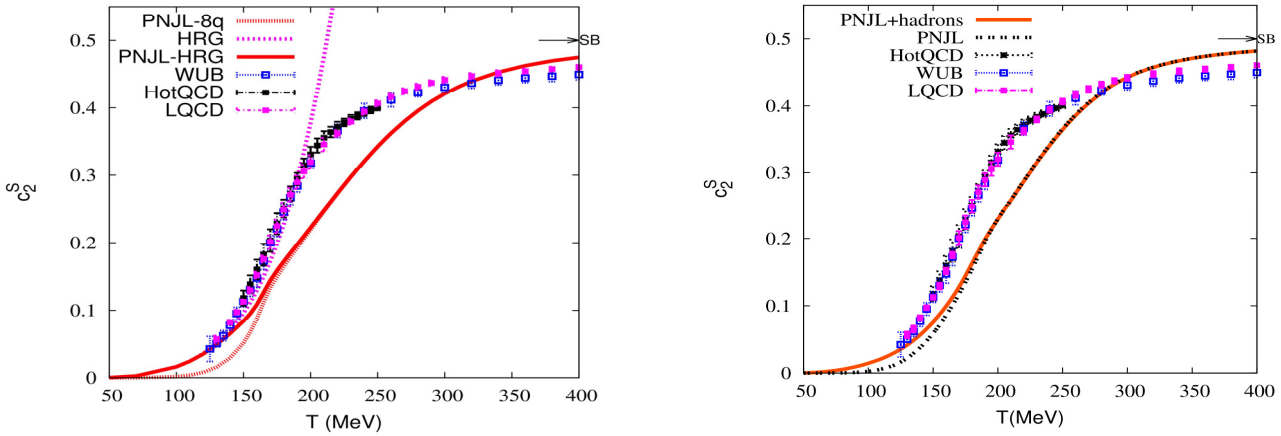


(**a**) (**b**)

Figure 9. Second-order charge fluctuations. as obtained from (**a**) 8–quark PNJL+HRG hybrid model [55] and (**b**) mass-modified PNJL model [122].

Similar situation occurs in the strange sector. In Figure 10, the HRG results show agreement to the lattice up to a higher temperature than the crossover one. One reason could be that HRG considers only the experimentally found hadrons, whereas the lattice can have contributions from additional strange hadrons predicted by theoretical quark

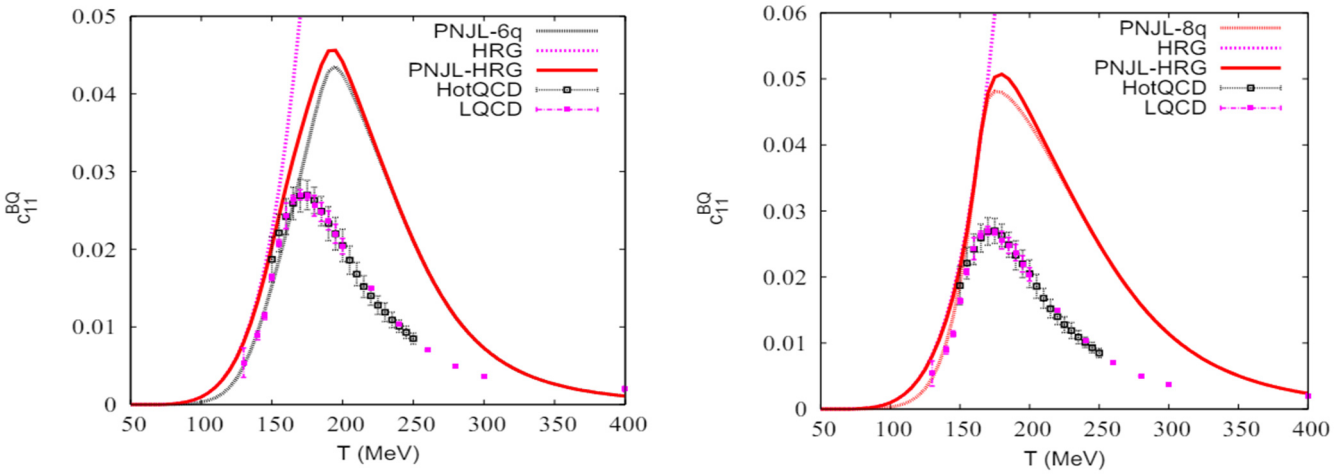
models. In the case of the mass-modified PNJL model, the contributions from the strange sector come from K and η, whose masses are still quite large. Also, the fact remains that constituent strange quark masses do not dilute as fast in the range of temperature where K-mass remains almost constant. The use of any higher-lying strange quark cannot resolve the issue. The artifact can therefore possibly be rectified, as reported in [122], by suitable reparameterization of the NJL part in the strange sector.



(**a**) (**b**)

Figure 10. Second-order strange fluctuations, as obtained from (**a**) 8–quark PNJL+HRG hybrid model [55] and (**b**) mass-modified PNJL model [122].

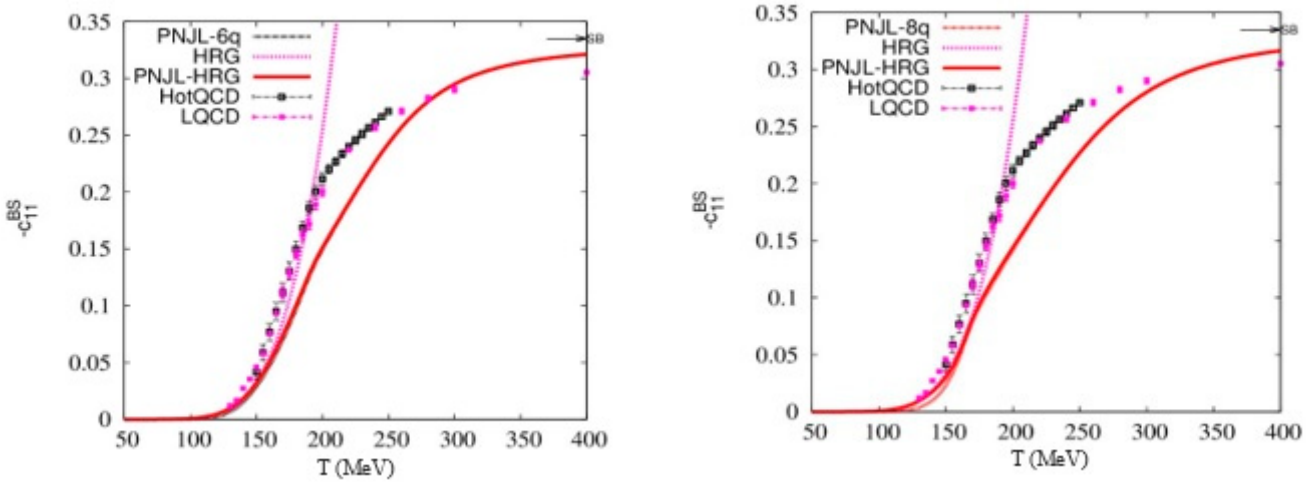
Among the leading-order correlations between the conserved charges, c_{11}^{BQ} is shown in Figure 11 for both six- and eight-quark-type interacting hybrid models. The baryon and electric charges remain correlated in the low-temperature regime, as the baryons and anti-baryons have positive and negative electric charges, respectively. Relatively large masses constrain the correlations at a low temperature. They then increase with temperature. But, as in the partonic phase, free quarks with small masses are produced, and the correlation again tends to zero. It therefore acquires a hump-like behavior for a model where transition is incorporated. The mismatch is anticipated to be occurring due to the slow dilution in the constituent masses of the charged strange quarks.



(**a**) (**b**)

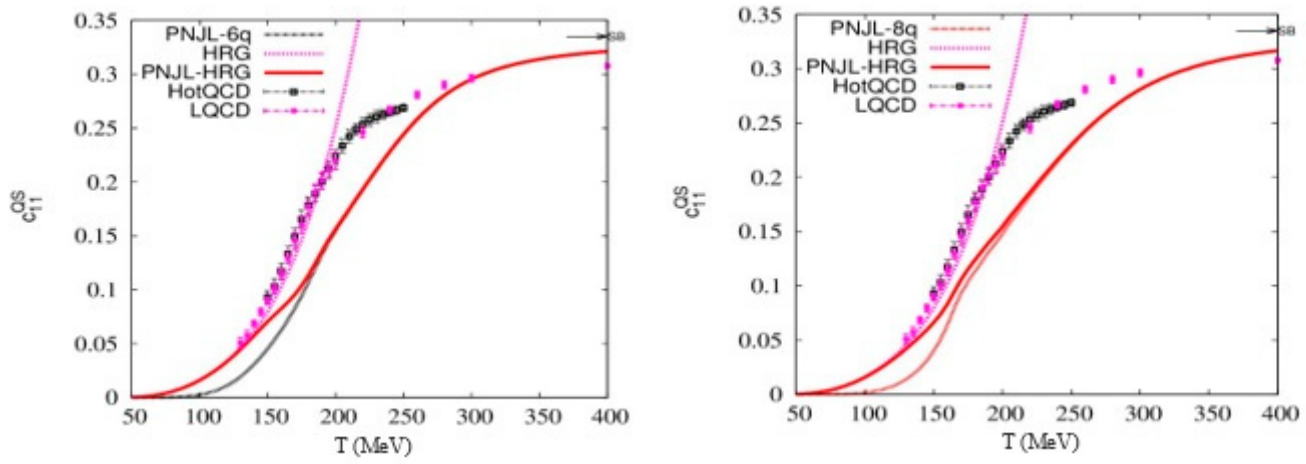
Figure 11. Leading-order Baryon number-charge correlations, as obtained from (**a**) 6–quark and (**b**) 8–quark PNJL model. Figures are taken from [55].

In Figure 12, the correlations between the baryon number and strangeness (BS) for a similar set up are shown, whereas Figure 13 projects the correlations for charge and strangeness (QS). As the contribution of light strange mesons is higher in QS, the correlation is also higher than BS in the intermediate range of temperature. The qualitative behavior is as per expectation from a model with in-between transition. The underestimation of BS and QS correlations of lattice data by the PNJL model is possibly due to the slow melting of the strange quark masses again.



(**a**) (**b**)

Figure 12. Leading-order Baryon number-strangeness correlations, as obtained from (**a**) 6-quark and (**b**) 8-quark PNJL model. Figures are taken from [55].



(**a**) (**b**)

Figure 13. Leading-order charge-strangeness correlations, as obtained from (**a**) 6–quark and (**b**) 8–quark PNJL model. Figures are taken from [55].

One of the primary causes for the mismatches found comes from the strange sector. This can be verified by examining corresponding quantities at the flavor level. It is also to be kept in mind that the strange particles also contribute to the related observations involving electric charge. Figure 14, displayed below, shows the justification. Some of these have been studied in [88].

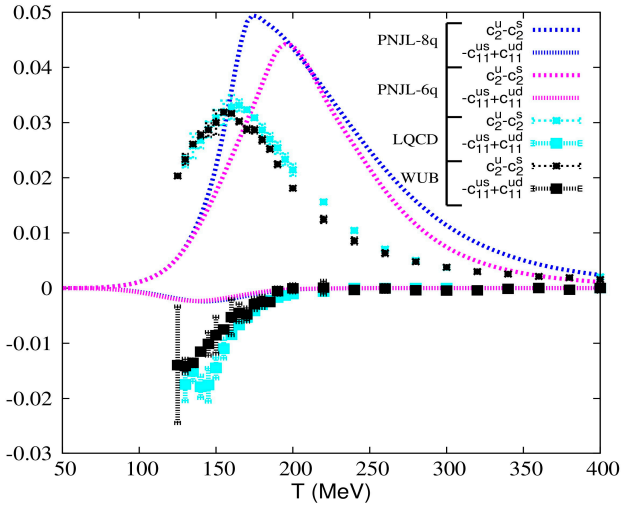


Figure 14. Fluctuations and correlations at the flavor level involving strange quarks from PNJL model with both 6–quark and 8–quark type interactions, compared with existing lattice results [40,42].

The parametrization in the model in its present version has a high current strange quark mass. The constituent mass of the strange quark thereby dilutes quite slowly and, at a high temperature, still acquires a higher mass than expected. This can be verified in Figure 15 below.

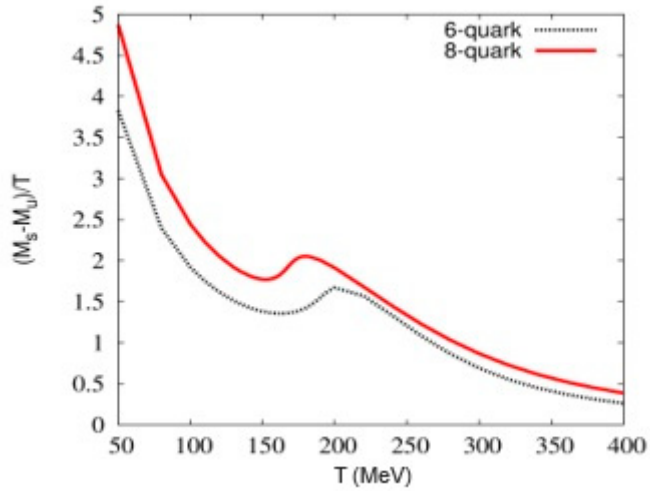


Figure 15. Strange constituent mass, scaled.

Non-monotonicity occurs, where the strange quark mass starts to fall more slowly as compared to the up quark mass. In the higher-temperature region as well, it possesses quite a high value. This suggests necessary rectification in the model parameterization with a lower current mass of the strange quark. The rectified framework, then coupled with the mass-modified version of the PNJL framework, can suitably describe the observables under concern. Moreover, the medium-mass modifications, as described, are performed under the mean-field scenario. Moving to the next level, incorporating the hadronic part of potential into the modifications of the degrees of freedom involved can lead to the closest proximity to the physical picture.

4. Conclusions

Among the various possible signatures of QGP production, studies of fluctuations and correlations among the conserved charges are very effective and efficient. To this end,

lattice QCD provides a benchmark theoretically. However, parallel studies of effective models need to be carried out for reasons manifold. The Polyakov-enhanced NJL (PNJL) model, in this regard, is very effective qualitatively. Quantitative accuracy, however, can be achieved once at least low-lying hadrons are incorporated suitably. Two methods to achieve this have been discussed here in parallel. The use of an external switching function behaving smoothly near the transition region can be made to join the HRG and PNJL results simultaneously, giving the necessary weightage corresponding to the applicable temperature domain. The thermodynamic variables and fluctuations of conserved charges now show a proper match near and below the crossover domain. The absence of suitable hadronic degrees of freedom in the low-temperature sector in the PNJL framework is thus solved in this first attempt by considering a mixture of degrees of freedom near the crossover. However, this method has its own difficulties arising from the approximation in its form. The switching function used in this study aims to choose the degrees of freedom adequately in the relevant region of corresponding phases without any overcounting in them. All the observables were considered to depend on the function independently, and hence, the dependence of the derivative terms is excluded after examination. Otherwise, the number of parameters would have been increasing, making the theory more dependent on effective fitting. Again, the applicability in the finite chemical potential domain can be of prime concern. The mismatch in the strange chemical potential, on the other hand, can be attributed to the slow melting of strange condensate in the PNJL model, which demands reparameterization in the sector. This becomes quite evident while studying the observables at the flavor level. The constituent masses of the strange quarks and, in particular, their slow dilution with increasing temperature, cause the problem. To conclude, this simplistic idea has worked quite well to reproduce the physics of strongly interacting matter, at the same time posing a few questions for further improvement toward quantitative accuracy. These issues now motivate building a more self-sustained model by using the medium-dependent masses of the hadrons, which can necessarily suppress the dominance of hadronic degrees of freedom in the higher-temperature region. Thus, the more elementary way, using medium-dependent hadronic masses and thereby including the potential, is introduced. These masses being generated while the system is evolving make the process a fundamental one. The susceptibilities and correlations are thus found to agree with the lattice result much better, as discussed. One major concern of the finite chemical potential in the earlier approach is now automatically addressed, as no additional fitting method is required here. The hadronic masses, being medium-dependent, can extrapolate themselves to choose dominant degrees of freedom that are relevant in the corresponding temperature window. There are, however, still some discrepancies remaining, accounting for some artifacts that need special attention. The masses are extracted by using mean-field values of the degrees of freedom associated. Once the entire thermodynamic potential can be minimized, the theory can somewhat mimic the beyond mean-field scenario, which is planned to be presented in the future.

Funding: S.U. is funded by the University Grant Commission and the Government of West Bengal. The work was not carried out presently under any particular project.

Data Availability Statement: The dataset has been made available upon discussions with authors.

Acknowledgments: The author deeply acknowledges the affiliating Institute for providing all necessary infrastructures. S.U. also thanks the collaborative authors KS, RR, SR, SKG, AB, SM, SG, SD, SS, and PD in corresponding works for the necessary discussions and help.

Conflicts of Interest: No conflict of interest is declared by the author. The funders played no role in designing the study; the generation and interpretation of data; or formatting the manuscript.

References

1. Boyd, G.; Engels, J.; Karsch, F.; Laermann, E.; Legeland, C.; Lugermeier, M.; Peterson, B. Thermodynamics of SU(3) lattice gauge theory. *Nucl. Phys. B* **1996**, *469*, 419–444. [CrossRef]
2. Engels, J.; Kaczmarek, O.; Karsch, F.; Laermann, E. The quenched limit of lattice QCD at non-zero baryon number. *Nucl. Phys. B* **1999**, *558*, 307–326. [CrossRef]
3. Fodor, Z.; Katz, S.D. A new method to study lattice QCD at finite temperature and chemical potential. *Phys. Lett. B* **2002**, *534*, 87–92. [CrossRef]
4. Fodor, Z.; Katz, S.D.; Szabo, K.K. The QCD equation of state at nonzero densities: Lattice result. *Phys. Lett. B* **2003**, *568*, 73–77. [CrossRef]
5. Allton, C.R.; Ejiri, S.; Hands, S.J.; Kaczmarek, O.; Karsch, F.; Laermann, E.; Schmidt, C.; Scorzato, L. QCD thermal phase transition in the presence of a small chemical potential. *Phys. Rev. D* **2002**, *66*, 074507. [CrossRef]
6. Bhattacharyya, A.; Das, S.; Ghosh, S.K.; Raha, S.; Ray, R.; Saha, K.; Upadhaya, S. Net Charge Fluctuations as a signal of QGP from Polyakov-Nambu-Jona-Lasinio model. *arXiv* **2012**, arXiv:1212.6010.
7. Jeon, S.; Koch, V. Fluctuations of Particle Ratios and the Abundance of Hadronic Resonances. *Phys. Rev. Lett.* **1999**, *83*, 5435. [CrossRef]
8. Jeon, S.; Koch, V. Charged Particle Ratio Fluctuation as a Signal for Quark-Gluon Plasma. *Phys. Rev. Lett.* **2000**, *85*, 2076–2079. [CrossRef]
9. Stock, R. Event by event analysis of ultrarelativistic nuclear collisions: A new method to search for critical fluctuations. In Proceedings of the NATO Advanced Study Workshop on Hot Hadronic Matter: Theory and Experiment, Divonne-les-Bains, France, 27 June–1 July 1994; Letessier, J., Gutbrod, H.H., Rafelski, J., Eds.; Plenum Press: New York, NY, USA, 1995.
10. Stephanov, M.; Rajagopal, K.; Shuryak, E. Event-by-event fluctuations in heavy ion collisions and the QCD critical point. *Phys. Rev. D* **1999**, *60*, 114028. [CrossRef]
11. Ding, H.-T.; Karsch, F.; Mukherjee, S. Thermodynamics of Strong-Interaction Matter from Lattice QCD. In *Quark Gluon Plasma 5*; Wang, X.N., Ed.; World Scientific: Singapore, 2016.
12. Pereira, R.C.; Costa, P. Building models of quarks and gluons with an arbitrary number of colors using Cartan-Polyakov loop. *Nucl. Phys. B* **2024**, *998*, 116415. [CrossRef]
13. Deb, P.; Varma, R. Fluctuations of conserved charges with finite size PNJL model. *arXiv* **2022**, arXiv:2209.06297.
14. Bühlmann, P.; Wenger, U. Heavy-dense QCD at fixed baryon number without a sign problem. In Proceedings of the ScienceVolume 396, 38th International Symposium on Lattice Field Theory, LATTICE 2021, Online, 26–30 July 2021; p. 584.
15. Bhattacharya, T.; Buchoff, M.I.; Christ, N.H.; Ding, H.T.; Gupta, R.; Jung, C.; Karsch, F.; Lin, Z.; Mawhinney, R.D.; McGlynn, G.; et al. QCD Phase Transition with Chiral Quarks and Physical Quark Masses. *Phys. Rev. Lett.* **2014**, *113*, 082001. [CrossRef]
16. Gottlieb, S.A.; Heller, U.M.; Kennedy, A.D.; Kim, S.; Kogut, J.B.; Liu, C.; Renken, R.L.; Sinclair, D.K.; Sugar, R.L.; Toussaint, D.; et al. Thermodynamics of lattice QCD with two light quark flavors on a 16**3 x 8 lattice. *2. Phys. Rev. D* **1997**, *55*, 6852–6860. [CrossRef]
17. Allton, C.R.; Ejiri, S.; Hands, S.J.; Kaczmarek, O.; Karsch, F.; Laermann, E.; Schmidt, C. Equation of state for two flavor QCD at nonzero chemical potential. *Phys. Rev. D* **2003**, *68*, 014507. [CrossRef]
18. de Forcrand, P.; Philipsen, O. The QCD phase diagram for three degenerate flavors and small baryon density. *Nucl. Phys. B* **2003**, *673*, 170–186. [CrossRef]
19. Aoki, Y.; Fodor, Z.; Katz, S.D.; Szabo, K.K. The QCD transition temperature: Results with physical masses in the continuum limit. *Phys. Lett. B* **2006**, *643*, 46–54. [CrossRef]
20. Aoki, Y.; Endrodi, G.; Fodor, Z.; Katz, S.D.; Szabo, K.K. The Order of the quantum chromodynamics transition predicted by the standard model of particle physics. *Nature* **2006**, *443*, 675–678. [CrossRef] [PubMed]
21. Aoki, Y.; Borsanyi, S.; Durr, S.; Fodor, Z.; Katz, S.D.; Krieg, S.; Szabo, K.K. The QCD transition temperature: Results with physical masses in the continuum limit II. *J. High Energy Phys.* **2009**, *06*, 088. [CrossRef]
22. Borsanyi, S.; Fodor, Z.; Katz, S.D.; Krieg, S.; Ratti, C.; Szabo, K.K. Freeze-Out Parameters: Lattice Meets Experiment. *Phys. Rev. Lett.* **2013**, *111*, 062005. [CrossRef] [PubMed]
23. Bazavov, A.; Bhattacharya, T.; Cheng, M.; DeTar, C.; Ding, H.T.; Gottlieb, S.; Gupta, R.; Hegde, P.; Heller, U.M.; Karsch, F.; et al. Chiral and deconfinement aspects of the QCD transition. *Phys. Rev. D* **2012**, *85*, 054503. [CrossRef]
24. Bazavov, A.; Bhattacharya, T.; DeTar, C.; Ding, H.T.; Gottlieb, S.; Gupta, R.; Hegde, P.; Heller, U.M.; Karsch, F.; Laermann, E.; et al. Equation of state in (2 + 1)-flavor QCD. *Phys. Rev. D* **2014**, *90*, 094503. [CrossRef]
25. Borsanyi, S.; Fodor, Z.; Hoelbling, C.; Katz, S.D.; Krieg, S.; Szabo, K.K. Full result for the QCD equation of state with 2 + 1 flavors. *Phys. Lett. B* **2014**, *730*, 99–104. [CrossRef]
26. Hatta, Y.; Stephanov, M.A. Proton-Number Fluctuation as a Signal of the QCD Critical End Point. *Phys. Rev. Lett.* **2003**, *91*, 102003, Erratum in *Phys. Rev. Lett.* **2003**, *91*, 129901. [CrossRef]
27. Gazdzicki, M.; Mrowczynski, S. A Method to study 'equilibration' in nucleus-nucleus collisions. *Z. Phys. C* **1992**, *54*, 127–132.
28. Ejiri, S.; Karsch, F.; Redlich, K. Hadronic fluctuations at the QCD phase transition. *Phys. Lett. B* **2006**, *633*, 275–282. [CrossRef]
29. Stephanov, M.A. Non-Gaussian fluctuations near the QCD critical point. *Phys. Rev. Lett.* **2009**, *102*, 032301. [CrossRef]
30. Meisinger, P.N.; Ogilvie, M.C. Chiral symmetry restoration and Z_N symmetry. *Phys. Lett. B* **1996**, *379*, 163–168. [CrossRef]
31. Fukushima, K. Chiral effective model with the Polyakov loop. *Phys. Lett. B* **2004**, *591*, 277–284. [CrossRef]

32. Ratti, C.; Thaler, M.A.; Weise, W. Phases of QCD: Lattice thermodynamics and a field theoretical model. *Phys. Rev. D* **2006**, *73*, 014019. [CrossRef]
33. Ghosh, S.K.; Mukherjee, T.K.; Mustafa, M.G.; Ray, R. Susceptibilities and speed of sound from PNJL model. *Phys. Rev. D* **2006**, *73*, 114007. [CrossRef]
34. Mukherjee, S.; Mustafa, M.G.; Ray, R. Thermodynamics of the Polyakov-Nambu-Jona-Lasinio model with nonzero baryon and isospin chemical potentials. *Phys. Rev. D* **2007**, *75*, 094015. [CrossRef]
35. Ciminale, M.; Gatto, R.; Ippolito, N.D.; Nardulli, G.; Ruggieri, M. Three flavor Nambu–Jona-Lasinio model with Polyakov loop and competition with nuclear matter. *Phys. Rev. D* **2008**, *77*, 054023. [CrossRef]
36. Shao, G.Y.; Tang, Z.D.; Di Toro, M.; Colonna, M.; Gao, X.Y.; Gao, N. Phase transition of strongly interacting matter with a chemical potential dependent Polyakov loop potential. *Phys. Rev. D* **2016**, *94*, 014008. [CrossRef]
37. Shao, G.Y.; Tang, Z.D.; Di Toro, M.; Colonna, M.; Gao, X.Y.; Gao, N.; Zhao, Y.L. Entanglement interaction and the phase diagram of strongly interacting matter. *Phys. Rev. D* **2015**, *92*, 114027. [CrossRef]
38. Ghosh, S.; Peixoto, T.C.; Roy, V.; Serna, F.E.; Krein, G. Shear and bulk viscosities of quark matter from quark-meson fluctuations in the Nambu–Jona-Lasinio model. *Phys. Rev. D* **2016**, *93*, 045205. [CrossRef]
39. Islam, C.A.; Majumder, S.; Haque, N.; Mustafa, M.G. Vector meson spectral function and dilepton production rate in a hot and dense medium within an effective QCD approach. *J. High Energy Phys.* **2015**, *1502*, 11. [CrossRef]
40. Bellwied, R.; Borsanyi, S.; Fodor, Z.; Katz, S.D.; Pasztor, A.; Ratti, C.; Szabo, K.K. Fluctuations and correlations in high temperature QCD. *Phys. Rev. D* **2015**, *92*, 114505. [CrossRef]
41. Bazavov, A.; Bhattacharya, T.; DeTar, C.E.; Ding, H.T.; Gottlieb, S.; Gupta, R.; Hegde, P.; Heller, U.M.; Karsch, F.; Laermann, E.; et al. Fluctuations and correlations of net baryon number, electric charge, and strangeness: A comparison of lattice QCD results with the hadron resonance gas model. *Phys. Rev. D* **2012**, *86*, 034509. [CrossRef]
42. Borsányi, S.; Fodor, Z.; Katz, S.D.; Krieg, S.; Ratti, C.; Szabó, K. Fluctuations of conserved charges at finite temperature from lattice QCD. *J. High Energy Phys.* **2012**, *1201*, 138. [CrossRef]
43. Bazavov, A.; Ding, H.T.; Hegde, P.; Kaczmarek, O.; Karsch, F.; Laermann, E.; Mukherjee, S.; Petreczky, P.; Schmidt, C.; Smith, D.; et al. Freeze-Out Conditions in Heavy Ion Collisions from QCD Thermodynamics. *Phys. Rev. Lett.* **2012**, *109*, 192302. [CrossRef]
44. Schmidt, C. QCD bulk thermodynamics and conserved charge fluctuations with HISQ fermions. (for the BNL-Bielefeld Collaboration). *J. Phys. Conf. Ser.* **2012**, *432*, 012013. [CrossRef]
45. Bazavov, A.; Ding, H.T.; Hegde, P.; Kaczmarek, O.; Karsch, F.; Laermann, E.; Maezawa, Y.; Mukherjee, S.; Ohno, H.; Petreczky, P.; et al. Strangeness at High Temperatures: From Hadrons to Quarks. *Phys. Rev. Lett.* **2013**, *111*, 082301. [CrossRef]
46. Braun-Munzinger, P.; Redlich, K.; Stachel, J. Particle Production in Heavy Ion Collisions. *arXiv* **2003**, arXiv:nucl-th/0304013.
47. Karsch, F.; Redlich, K.; Tawfik, A. Thermodynamics at Non-Zero Baryon Number Density: A Comparison of Lattice and Hadron Resonance Gas Model Calculations. *Phys. Lett. B* **2003**, *571*, 67–74. [CrossRef]
48. Tawfik, A. QCD phase diagram: A comparison of lattice and hadron resonance gas model calculations. *Phys. Rev. D* **2005**, *71*, 054502. [CrossRef]
49. Andronic, A.; Braun-Munzinger, P.; Stachel, J.; Winn, M. Interacting hadron resonance gas meets lattice QCD. *Phys. Lett. B* **2012**, *718*, 80–85. [CrossRef]
50. Huovinen, P.; Petreczky, P. Hadron resonance gas with repulsive interactions and fluctuations of conserved charges. *Phys. Lett. B* **2018**, *777*, 125–130. [CrossRef]
51. Dashen, R.; Ma, S.-K.; Bernstein, H.J. *S*-Matrix Formulation of Statistical Mechanics. *Phys. Rev.* **1969**, *187*, 345–370. [CrossRef]
52. Dashen, R.; Ma, S.-K. Scattering Theory and Current Correlations in Classical Gases. *Phys. Rev. A* **1971**, *4*, 700. [CrossRef]
53. Braun-Munzinger, P.; Stachel, J.; Wessels, J.; Xu, N. Thermal equilibration and expansion in nucleus-nucleus collisions at the AGS. *Phys. Lett. B* **1995**, *344*, 43–48. [CrossRef]
54. Cleymans, J.; Elliott, D.; Satz, H.; Thews, R.L. Thermal hadron production in Si-Au collisions. *Z. Für Phys. C Part. Fields* **1997**, *74*, 319–323. [CrossRef]
55. Bhattacharyya, A.; Ghosh, S.K.; Maity, S.; Raha, S.; Ray, R.; Saha, K.; Samanta, S.; Upadhaya, S. Thermodynamics of strongly interacting matter in a hybrid model. *Phys. Rev. C* **2019**, *99*, 045207. [CrossRef]
56. Schaefer, B.-J.; Wambach, J. Susceptibilities near the QCD (tri)critical point. *Phys. Rev. D* **2007**, *75*, 085015. [CrossRef]
57. Scavenius, O.; Mócsy, Á.; Mishustin, I.N.; Rischke, D.H. Chiral phase transition within effective models with constituent quarks. *Phys. Rev. C* **2001**, *64*, 045202. [CrossRef]
58. Schaffner-Bielich, J. Effective Restoration of the $U_A(1)$ Symmetry in the SU(3) Linear σ Model. *Phys. Rev. Lett.* **2000**, *84*, 3261. [CrossRef] [PubMed]
59. Gupta, U.S.; Tiwari, V.K. Meson masses and mixing angles in the 2 + 1 flavor Polyakov quark meson sigma model and symmetry restoration effects. *Phys. Rev. D* **2010**, *81*, 054019. [CrossRef]
60. Tawfik, A.; Magdy, N.; Diab, A. Polyakov linear SU(3) σ model: Features of higher-order moments in a dense and thermal hadronic medium. *Phys. Rev. C* **2014**, *89*, 055210. [CrossRef]
61. Tawfik, A.N.; Diab, A.M.; Hussein, M.T. Quark-hadron phase structure, thermodynamics and magnetization of QCD matter. *arXiv* **2018**, arXiv:1604.08174. [CrossRef]
62. Tawfik, A.N.; Diab, A.M.; Ghoneim, M.T.; Anwer, H. SU(3) Polyakov linear-sigma model with finite isospin asymmetry: QCD phase diagram. *Eur. J. Mod. Phys. A* **2019**, *34*, 1950199. [CrossRef]

63. Tawfik, A.N.; Greiner, C.; Diab, A.M.; Ghoneim, M.T.; Anwer, H. Polyakov linear-σ model in mean-field approximation and optimized perturbation theory. *Phys. Rev. C* **2020**, *101*, 035210. [CrossRef]
64. Tawfik, A.N.; Diab, A.M. Chiral magnetic properties of QCD phase-diagram. *Eur. Phys. J. A* **2021**, *57*, 200. [CrossRef]
65. Tawfik, A.N. QCD Phase Structure and In-Medium Modifications of Meson Masses in Polyakov Linear-Sigma Model with Finite Isospin Asymmetry. *Universe* **2023**, *9*, 276. [CrossRef]
66. Tawfik, A.N.; Dabash, T.F.; Elshehri, A. Singularity attenuation with quantum-mechanically revised metric tensor. *Astron. Nachr.* **2024**, *345*, e240004. [CrossRef]
67. Ayala, A.; Bashir, A.; Dominguez, C.A.; Gutierrez, E.; Loewe, M. QCD phase diagram from finite energy sum rules. *Phys. Rev. D* **2011**, *84*, 056004. [CrossRef]
68. Gutierrez, E.; Ahmad, A.; Ayala, A.; Bashir, A.; Raya, A. The QCD phase diagram from Schwinger–Dyson equations. *J. Phys. G* **2014**, *41*, 075002. [CrossRef]
69. Contant, R.; Huber, M.Q. Phase structure and propagators at nonvanishing temperature for QCD and QCD-like theories. *Phys. Rev. D* **2017**, *96*, 074002. [CrossRef]
70. Ahmad, A. Chiral symmetry restoration and deconfinement in the contact interaction model of quarks with parallel electric and magnetic fields. *Chin. Phys. C* **2021**, *45*, 073109. [CrossRef]
71. Ahmad, A.; Bashir, A.; Dedolla, M.A.; Cobos-Martinez, J.J. Flavor, temperature and magnetic field dependence of the QCD phase diagram: Magnetic catalysis and its inverse. *J. Phys. G* **2021**, *487*, 075002. [CrossRef]
72. Ahmad, A.; Farooq, A. Schwinger Pair Production in QCD from Flavor-Dependent Contact Interaction Model of Quarks. *arXiv* **2023**, arXiv:2302.13265.
73. Ahmad, A.; Azher, M.; Raya, A. Robust features of a QCD phase diagram through a contact interaction model for quarks: A view from the effective potential. *Eur. Phys. J. A* **2023**, *59*, 252. [CrossRef]
74. Bhattacharyya, A.; Ghosh, S.K.; Ray, R.; Saha, K.; Upadhaya, S. Polyakov–Nambu–Jona-Lasinio model in finite volumes. *Eur. Phys. Lett.* **2016**, *116*, 52001. [CrossRef]
75. Ghosh, S. Electrical conductivity of hadronic matter from different possible mesonic and baryonic loops. *Phys. Rev. D* **2017**, *95*, 036018. [CrossRef]
76. Ghosh, S.; Ghosh, S.; Bhattacharyya, S. Phenomenological bound on the viscosity of the hadron resonance gas. *Phys. Rev. C* **2018**, *98*, 045202. [CrossRef]
77. Saha, K.; Ghosh, S.; Upadhaya, S.; Maity, S. Transport coefficients in a finite volume Polyakov–Nambu–Jona-Lasinio model. *Phys. Rev. D* **2018**, *97*, 116020. [CrossRef]
78. Singha, P.; Abhishek, A.; Kadam, G.; Ghosh, S.; Mishra, H. Calculations of shear, bulk viscosities and electrical conductivity in the Polyakov-quark–meson model. *J. Phys. G* **2019**, *46*, 015201. [CrossRef]
79. Ghosh, S.; Ghosh, S. One-loop Kubo estimations of the shear and bulk viscous coefficients for hot and magnetized bosonic and fermionic systems. *Phys. Rev. D* **2021**, *103*, 096015. [CrossRef]
80. Islam, C.A.; Mustafa, M.G.; Ray, R.; Singha, P. Consistent approach to study gluon quasiparticles. *Phys. Rev. D* **2022**, *106*, 054002. [CrossRef]
81. Elze, H.T.; Greiner, W. Finite Size Effects for Quark—Gluon Plasma Droplets. *Phys. Lett. B* **1986**, *179*, 385–392. [CrossRef]
82. Hua, L.M.; Xu, J. Shear viscosity of nuclear matter in the spinodal region. *Phys. Rev. C* **2023**, *107*, 034601. [CrossRef]
83. Saha, K. Theoretical Perspectives on Viscous Nature of Strongly Interacting Systems. *Universe* **2024**, *10*, 259. [CrossRef]
84. Bhattacharyya, A.; Deb, P.; Lahiri, A.; Ray, R. Susceptibilities with multi-quark interactions in PNJL model. *Phys. Rev. D* **2010**, *82*, 114028. [CrossRef]
85. Bhattacharyya, A.; Deb, P.; Lahiri, A.; Ray, R. Correlation between conserved charges in PNJL Model with multi-quark interactions. *Phys. Rev. D* **2011**, *83*, 014011. [CrossRef]
86. Ghosh, S.K.; Mukherjee, T.K.; Mustafa, M.G.; Ray, R. Polyakov-Nambu-Jona-Lasinio model with a Vandermonde term. *Phys. Rev. D* **2008**, *77*, 094024. [CrossRef]
87. Bhattacharyya, A.; Deb, P.; Ghosh, S.K.; Ray, R. Investigation of the phase diagram and bulk thermodynamic properties using the Polyakov–Nambu–Jona-Lasinio model with eight-quark interactions. *Phys. Rev. D* **2010**, *82*, 014021. [CrossRef]
88. Bhattacharyya, A.; Ghosh, S.K.; Maity, S.; Raha, S.; Ray, R.; Saha, K.; Upadhaya, S. Reparametrizing the Polyakov–Nambu–Jona-Lasinio model. *Phys. Rev. D* **2017**, *95*, 054005. [CrossRef]
89. Jeon, S.; Koch, V.; Hwa, R.C. Event-by-Event Fluctuations; Quark gluon plasma. *arXiv* **2003**, arXiv:hep-ph/0304012.
90. Kumar, D.; Sarkar, N.; Bhaduri, P.P.; Jaiswal, A. Examination of thermalization of quarkonia at energies available at the CERN Large Hadron Collider. *Phys. Rev. C* **2023**, *107*, 064906.
91. Braun-Munzinger, P.; Stachel, J. Production of strange clusters and strange matter in nucleus-nucleus collisions at the AGS. *J. Phys. G* **1995**, *21*, L17–L20. [CrossRef]
92. Braun-Munzinger, P.; Heppe, I.; Stachel, J. Chemical equilibration in Pb+Pb collisions at the SPS. *Phys. Lett. B* **1999**, *465*, 15–20. [CrossRef]
93. Cleymans, J.; Redlich, K. Chemical and thermal freeze-out parameters from **1A** to **200A** GeV. *Phys. Rev. C* **1999**, *60*, 054908. [CrossRef]
94. Braun-Munzinger, P.; Magestro, D.; Redlich, K.; Stachel, J. Hadron production in Au–Au collisions at RHIC. *Phys. Lett. B* **2001**, *518*, 41–46. [CrossRef]

95. Xu, N.; Kaneta, M. Hadron freeze-out conditions in high energy nuclear collisions. *Nucl. Phys. A* **2002**, *698*, 306–313. [CrossRef]
96. Becattini, F.; Manninen, J.; Gazdzicki, M. Energy and system size dependence of chemical freeze-out in relativistic nuclear collisions. *Phys. Rev. C* **2006**, *73*, 044905. [CrossRef]
97. Andronic, A.; Braun-Munzinger, P.; Stachel, J. Hadron production in central nucleus-nucleus collisions at chemical freeze-out. *Nucl. Phys. A* **2006**, *772*, 167–199. [CrossRef]
98. Cleymans, J.; Oeschler, H.; Redlich, K.; Wheaton, S. Comparison of chemical freeze-out criteria in heavy-ion collisions. *Phys. Rev. C* **2006**, *73*, 034905. [CrossRef]
99. Andronic, A.; Braun-Munzinger, P.; Stachel, J. Thermal hadron production in relativistic nuclear collisions: The hadron mass spectrum, the horn, and the QCD phase transition. *Phys. Lett. B* **2009**, *673*, 142–145. [CrossRef]
100. Andronic, A.; Braun-Munzinger, P.; Stachel, J. The horn, the hadron mass spectrum and the QCD phase diagram—The statistical model of hadron production in central nucleus-nucleus collisions. *Nucl. Phys. A* **2010**, *834*, 237c–240c. [CrossRef]
101. Koch, V.; Bleicher, M.; Jeon, S. Event-by-event fluctuations and the QGP. *Nucl. Phys. A* **2002**, *698*, 261–268. [CrossRef]
102. Chatterjee, S.; Das, S.; Kumar, L.; Mishra, D.; Mohanty, B.; Sahoo, R.; Sharma, N. Freeze-Out Parameters in Heavy-Ion Collisions at AGS, SPS, RHIC, and LHC Energies. *Adv. High Energy Phys.* **2015**, *2015*, 349013. [CrossRef]
103. Bhattacharyya, A.; Ghosh, S.K.; Ray, R.; Samanta, S. Exploring effects of magnetic field on the Hadron Resonance Gas. *Euro. Phys. Lett.* **2016**, *115*, 62003. [CrossRef]
104. Bollweg, D.; Goswami, J.; Kaczmarek, O.; Karsch, F.; Mukherjee, S.; Petreczky, P.; Schmidt, C.; Scior, P.; HotQCD Collaboration. Second order cumulants of conserved charge fluctuations revisited: Vanishing chemical potentials. *Phys. Rev. D* **2021**, *104*, 074512.
105. Bhattacharyya, A.; Das, S.; Ghosh, S.K.; Ray, R.; Samanta, S. Fluctuations and correlations of conserved charges in an excluded-volume hadron resonance gas model. *Phys. Rev. C* **2014**, *90*, 034909. [CrossRef]
106. Sahoo, B.; Pradhan, K.K.; Sahu, D.; Sahoo, R. Effect of a magnetic field on the thermodynamic properties of a high-temperature hadron resonance gas with van der Waals interactions. *Phys. Rev. D* **2023**, *108*, 074028. [CrossRef]
107. Hagedorn, R.; Rafelski, J. Hot hadronic matter and nuclear collisions. *Phys. Lett. B* **1980**, *97*, 136–142. [CrossRef]
108. Rischke, D.H.; Gorenstein, M.I.; Stöcker, H.; Greiner, W. Excluded volume effect for the nuclear matter equation of state. *Z. Für Phys. C Part. Fields* **1991**, *51*, 485–489. [CrossRef]
109. Cleymans, J.; I Gorenstein, M.; Stålnacke, J.; Suhonen, E. Excluded volume effect and the quark-hadron phase transition. *Phys. Scr.* **1993**, *48*, 277–280. [CrossRef]
110. Singh, C.; Patra, B.; Singh, K. Thermodynamically consistent EOS for hot dense hadron gas. *Phys. Lett. B* **1996**, *387*, 680–684. [CrossRef]
111. Yen, G.D.; Gorenstein, M.I.; Greiner, W.; Yang, S.N. Excluded volume hadron gas model for particle number ratios in *A+A* collisions. *Phys. Rev. C* **1997**, *56*, 2210. [CrossRef]
112. Gorenstein, M.I.; Hauer, M.; Moroz, O.N. Viscosity in the excluded volume hadron gas model. *Phys. Rev. C* **2008**, *77*, 024911. [CrossRef]
113. Fu, J. Statistical model analysis of particle ratio fluctuations in heavy-ion collisions. *Phys. Rev. C* **2012**, *85*, 064905. [CrossRef]
114. Begun, V.V.; Gazdzicki, M.; Gorenstein, M.I. Hadron-resonance gas at freeze-out: Reminder on the importance of repulsive interactions. *Phys. Rev. C* **2013**, *88*, 024902. [CrossRef]
115. Fu, J. Higher moments of net-proton multiplicity distributions in heavy ion collisions at chemical freeze-out. *Phys. Lett. B* **2013**, *722*, 144–150. [CrossRef]
116. Tawfik, A. Constant-trace anomaly as a universal condition for the chemical freeze-out. *Phys. Rev. C* **2013**, *88*, 035203. [CrossRef]
117. Hama, Y.; Kodama, T.; Socolowski, O. Topics on Hydrodynamic Model of Nucleus-Nucleus Collisions. *Braz. J. Phys.* **2005**, *35*, 24–51. [CrossRef]
118. Werner, K.; Karpenko, I.; Pierog, T.; Bleicher, M.; Mikhailov, K. Event-by-event simulation of the three-dimensional hydrodynamic evolution from flux tube initial conditions in ultrarelativistic heavy ion collisions. *Phys. Rev. C* **2010**, *82*, 044904. [CrossRef]
119. Merdeev, A.V.; Satarov, L.M.; Mishustin, I.N. Hydrodynamic modeling of the deconfinement phase transition in heavy-ion collisions in the NICA–FAIR energy domain. *Phys. Rev. C* **2011**, *84*, 014907. [CrossRef]
120. Olive, K.A. Review of Particle Physics. (Particle Data Group). *Chin. Phys. C* **2014**, *38*, 090001. [CrossRef]
121. Abelev, B.; Adam, J.; Adamova, D.; Adare, A.M.; Aggarwal, M.M.; Aglieri Rinella, G.; Agocs, A.G.; Agostinelli, A.; Aguilar Salazar, S.; Ahammed, Z.; et al. Net-Charge Fluctuations in Pb-Pb Collisions at $\sqrt{S_{NN}}$=2.76 TeV. *Phys. Rev. Lett.* **2013**, *110*, 152301. [CrossRef]
122. Bhattacharyya, A.; Deb, P.; Ghosh, S.K.; Maity, S.; Raha, S.; Ray, R.; Saha, K.; Upadhaya, S. Finite temperature properties of a modified Polyakov–Nambu–Jona-Lasinio model. *Phys. Rev. D* **2020**, *102*, 074006. [CrossRef]
123. Karsch, F.; Redlich, K. Probing freeze-out conditions in heavy ion collisions with moments of charge fluctuations. *Phys. Lett. B* **2011**, *695*, 136–142. [CrossRef]
124. Albright, M.; Kapusta, J.; Young, C. Matching excluded-volume hadron-resonance gas models and perturbative QCD to lattice calculations. *Phys. Rev. C* **2014**, *90*, 024915. [CrossRef]
125. Miyahara, A.; Torigoe, Y.; Kouno, H.; Yahiro, M. Equation of state and transition temperatures in the quark-hadron hybrid model. *Phys. Rev. D* **2016**, *94*, 016003. [CrossRef]
126. Miyahara, A.; Ishii, M.; Kouno, H.; Yahiro, M. Crossover-model approach to QCD phase diagram, equation of state and susceptibilities in the 2 + 1 and 2 + 1 + 1 flavor systems. *Int. J. Mod. Phys. A* **2017**, *32*, 1750205. [CrossRef]

127. Yukalov, V.I.; Yukalova, E.P. Multichannel approach to clustering matter. *Physica A* **1997**, *243*, 382–414. [CrossRef]
128. Yukalov, V.I.; Yukalova, E.P. Thermodynamics of strong interactions. *Phys. Part. Nucl.* **1997**, *28*, 37. [CrossRef]
129. Yukalov, V.I.; Yukalova, E.P. Models of Mixed Matter. *Phys. Part. Nucl.* **2023**, *54*, 1–68. [CrossRef]
130. Yukalov, V.I.; Yukalova, E. Phase transition in multicomponent field theory at finite temperature. *arXiv* **2015**, arXiv:1502.07109.
131. Yukalov, V.I.; Yukalova, E.P. Calculation of critical exponents by self-similar factor approximants. *Eur. Phys. J. B* **2007**, *55*, 93–99. [CrossRef]

Disclaimer/Publisher's Note: The statements, opinions and data contained in all publications are solely those of the individual author(s) and contributor(s) and not of MDPI and/or the editor(s). MDPI and/or the editor(s) disclaim responsibility for any injury to people or property resulting from any ideas, methods, instructions or products referred to in the content.